

Finite element formulations for 3D convex polyhedra in nonlinear continuum mechanics

Markus Kraus, Paul Steinmann

Chair of Applied Mechanics, University Erlangen-Nuremberg

Egerlandstrasse 5, 91058 Erlangen, Germany

e-mail: markus.kraus@ltm.uni-erlangen.de, paul.steinmann@ltm.uni-erlangen.de

In this paper, we present finite element formulations for general three-dimensional convex polyhedra for use in a common finite element framework that are well suited, e.g., for modeling complex granular materials and for mesh refinements. Based on an universally applicable interpolant for any convex polyhedron, different interpolation schemes are investigated in the context of nonlinear elastostatics.

The modeling benefits and the numerical performance regarding the mechanical response and the computational cost are analyzed by several examples.

Keywords: nonlinear finite elements, polyhedral elements, 3D interpolation, finite elasticity

1. INTRODUCTION

For today's simulations the finite element method is a very powerful and well-established method for the approximate solution of partial differential equations. The known standard element formulations are very robust and efficient at low computational costs, but usually limited to simple geometries like triangles and quadrilaterals in 2D and tetrahedra and hexahedra in 3D, respectively. In this paper we aim at extending the available element geometries to arbitrary convex polyhedra in 3D.

This new class of polyhedral finite elements is very powerful for different applications. Providing great flexibility for technical meshing problems, these elements may cover a huge range from structured polyhedra, e.g., for mesh refinements (Fig. 1a), up to complete random crystalline shapes mimicking polycrystalline granular microstructures (Fig. 1b). Those structural characterizations of real grains may be obtained, e.g., by a focused ion beam-scanning electron microscope (FIB-SEM, [5, 6]) or computed tomography (CT, [23]). Polyhedral elements can also be applied onto optimal meshes generated by the adaptive Delaunay tessellation (ADT) proposed by Constantiniu et al. [2]. An additional benefit of our polyhedral elements is the enclosed formulation on the element level leaving the surrounding finite element discretization unaffected by, e.g., suppressing multi-point constraints for hanging nodes.

Due to the unavailability of analytic shape functions for arbitrary polyhedra, alternative interpolation schemes are necessary. For irregularly scattered datasets, many mesh and element-free interpolation schemes exist in the field of scientific visualization. The most known group is formed by natural neighbor interpolations proposed by Sibson [16, 17] that have been modified by Watson [28]. Sibson interpolations were first introduced by Traversoni [22] and Sambridge et al. [14] in the Galerkin-type natural neighbor, also known as natural element method (NEM), extended by Sukumar et al. for continuum mechanical problems [19, 20]. A different approach named Laplacian and non-Sibson interpolants were used by Belikov et al. [1] and Hiyoshi and Sugihara [7], respectively. The polygonal finite element interpolants developed independently by Sukumar and

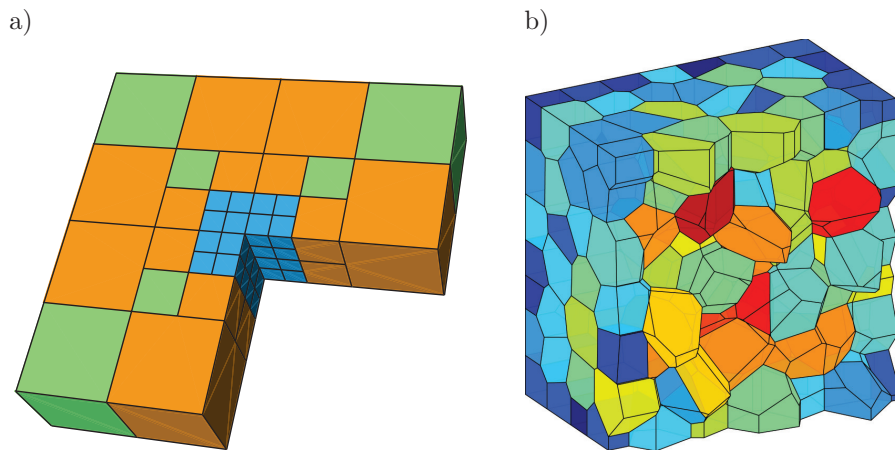


Fig. 1. Applications for polyhedral finite elements: a) transition elements for mesh refinement near singularities (color indicating nodes per element: 8 (blue), 9 (green), 13 (orange)), b) granular material discretization (8 (dark blue)-38 (dark red) nodes per element).

Tabarraei [21] and Sukumar and Malsch [18] are also based on the Laplacian and non-Sibson interpolation.

Another group are generalized barycentric coordinates, for which the first fundamental idea for the usage in a finite element framework was already made by Wachspress [24]. Generalized rational barycentric coordinates on arbitrary polygons and polyhedra have been developed, generalized and analyzed in the works of Warren [25, 26], Meyer et al. [11], Floater et al. [4, 8], Lipman [9], and Warren et al. [27]. A very general approach for the construction of 2D interpolants has been presented by Malsch and Dasgupta [3, 10] that are also suitable for non-convex domains with holes.

On the topic of two-dimensional polygonal finite elements Sukumar et al. [21] have contributed significant work, and also boundary element based approaches exist on polygons, see, e.g., Weißer [29].

2. PROBLEM DESCRIPTION

We consider a general nonlinear elastic problem for 3D continua, Fig. 2.

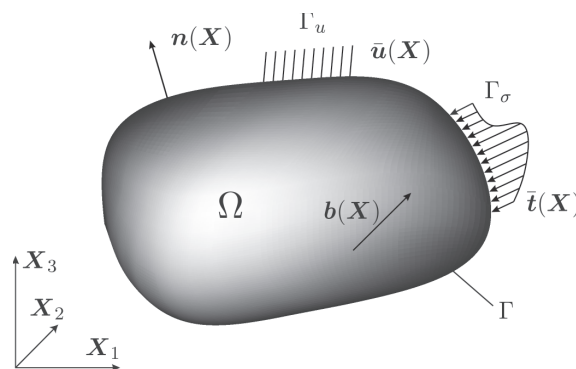


Fig. 2. 3D elastic body.

Its weak form and finite element discretization is based on the equality of the internal and external virtual work $\delta W_{\text{int}} = \delta W_{\text{ext}}$. We describe our problem in the reference configuration, thus with the deformation gradient

$$\mathbf{F} = \frac{\partial \mathbf{x}}{\partial \mathbf{X}} = \mathbf{I} + \frac{\partial \mathbf{u}}{\partial \mathbf{X}} \quad (1)$$

we obtain the internal and external virtual work in terms of the Green-Lagrange strain $\mathbf{E} = \frac{1}{2} [\mathbf{F}^T \mathbf{F} - \mathbf{I}]$ and the second Piola-Kirchhoff stress tensor \mathbf{S} as

$$\delta W_{\text{int}} = \int_{\Omega} \delta \mathbf{E} : \mathbf{S} \, d\Omega \quad (2)$$

and

$$\delta W_{\text{ext}} = \int_{\Omega} \rho \delta \mathbf{u} \cdot \mathbf{b} \, d\Omega + \int_{\Gamma_{\sigma}} \delta \mathbf{u} \cdot \bar{\mathbf{t}} \, d\Gamma \quad (3)$$

with the virtual displacements $\delta \mathbf{u}$, the prescribed displacements $\bar{\mathbf{u}}$ on the Dirichlet boundary Γ_u , the external surface stresses $\bar{\mathbf{t}}$ on the Neumann boundary Γ_{σ} , and the body forces \mathbf{b} .

Together with the constitutive equation $\mathbf{S} = \mathbf{S}(\mathbf{E})$ and the material tangent operator

$$\mathbb{C} = \frac{\partial \mathbf{S}}{\partial \mathbf{E}}, \quad (4)$$

the problem is closed.

Considering an isoparametric displacement-based discretization into n_e elements,

$$\Omega = \bigcup_{e=1}^{n_e} \Omega_e, \quad (5)$$

and with the still to be determined shape functions N^I for the I element nodes, the variation $\delta \mathbf{E}$ in (2) can be arranged in Voigt notation in terms of the \mathbf{B}^I -matrix,

$$\mathbf{B}^I = \begin{bmatrix} F_{11}N_{,1}^I & F_{21}N_{,1}^I & F_{31}N_{,1}^I \\ F_{12}N_{,2}^I & F_{22}N_{,2}^I & F_{32}N_{,2}^I \\ F_{13}N_{,3}^I & F_{23}N_{,3}^I & F_{33}N_{,3}^I \\ F_{11}N_{,2}^I + F_{12}N_{,1}^I & F_{21}N_{,2}^I + F_{22}N_{,1}^I & F_{31}N_{,2}^I + F_{32}N_{,1}^I \\ F_{12}N_{,3}^I + F_{13}N_{,2}^I & F_{22}N_{,3}^I + F_{23}N_{,2}^I & F_{32}N_{,3}^I + F_{33}N_{,2}^I \\ F_{13}N_{,1}^I + F_{11}N_{,3}^I & F_{23}N_{,1}^I + F_{21}N_{,3}^I & F_{33}N_{,1}^I + F_{31}N_{,3}^I \end{bmatrix}, \quad (6)$$

where $N_{,i}^I = \frac{\partial N^I}{\partial X_i}$ with $i = 1, 2, 3$, as

$$\delta \hat{\mathbf{E}} = \mathbf{B}^I \delta \mathbf{u}^I. \quad (7)$$

With the corresponding second Piola-Kirchhoff stresses $\hat{\mathbf{S}}$ in Voigt notation, this leads to the element's internal nodal force vector

$$\mathbf{f}_{\text{int}}^I = \int_{\Omega_e} \mathbf{B}^I \hat{\mathbf{S}} \, d\Omega_e. \quad (8)$$

The linearization of (8) results in the associated local tangential stiffness

$$\mathbf{K}^{IJ} = \int_{\Omega_e} \left[\frac{\partial N^I}{\partial \mathbf{X}} \cdot \mathbf{S} \cdot \frac{\partial N^J}{\partial \mathbf{X}} \mathbf{I} + [\mathbf{B}^I]^T \hat{\mathbb{C}} \mathbf{B}^J \right] d\Omega_e, \quad (9)$$

which is needed for the iterative solution of the nonlinear system of equations.

3. POLYHEDRON CONNECTIVITIES

Standard conventions for the representation of elements are only available for a few special polyhedral configurations, e.g., hexahedra or tetrahedra. In contrast to two-dimensional polygons, where we can simply settle a clockwise or counter-clockwise numbering of the nodes for any polygon, the description of arbitrary 3D polyhedra is more challenging, as there are no limitations or rules for the connectivities between nodes, edges and facets. For an arbitrary convex polyhedron, Fig. 3, the set \mathcal{X}^I consists of all polyhedral nodes \mathbf{X}^J that are connected by flat facets with the node \mathbf{X}^I . The set \mathcal{F}^I includes all adjacent facets F to node \mathbf{X}^I with the cardinality $n^I = \#\mathcal{F}^I$, see Fig. 4a. For the node-to-facet connectivities we apply a polygonal counter-clockwise numbering with respect to the associated outward pointing polar facet normal vector \mathbf{n}^F .

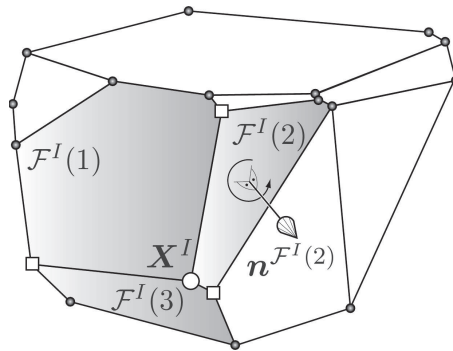


Fig. 3. Sets of polyhedral representation for the node \mathbf{X}^I : connected nodes in \mathcal{X}^I indicated with squares, adjacent facets in \mathcal{F}^I shaded, counter-clockwise node numbering on each facet (here shown for $\mathcal{F}^I(2)$).

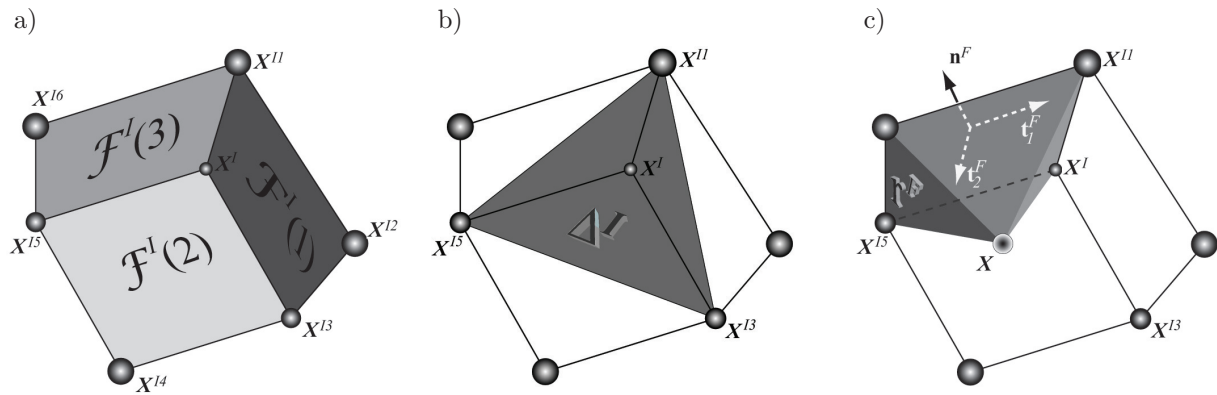


Fig. 4. Geometric connectivities and measures for node \mathbf{X}^I and evaluation point \mathbf{X} : a) nomenclature of adjacent facets for node I , b) nodal volume $\Delta^I(\mathcal{F}^I)$, c) point-to-facet volume r^F .

With the facet-to-node connectivities \mathcal{F}^I a classification of polyhedra is possible. We obtain for

$$\max(n^I) \begin{cases} = 3 & \text{simple} \\ > 3 & \text{complex} \end{cases} \quad (10)$$

polyhedra. As we do not limit our approach to simple polyhedra, we have to cope with the problems caused by complex polyhedra for three dimensional interpolants.

In the following sections, superscribed Roman letters indicate a variable directly linked to a node I or a facet F , calligraphic letters belong to geometric sets like sets of the adjacent facets. Index notation for spatial components of vectors and tensors are usually avoided by the usage of bold and bold capital letters, respectively.

4. GENERAL THREE-DIMENSIONAL INTERPOLANT ON ARBITRARY POLYHEDRA

The challenge for the creation of polyhedral elements is to gain control of how to interpolate given nodal values inside a convex polyhedral domain.

4.1. General Interpolation Properties

In any domain, the function value at an interior point is evaluated as the sum of the weighted function values f at the given discrete nodes \mathbf{X}^I ,

$$f(\mathbf{X}) = \sum_I N^I(\mathbf{X})f(\mathbf{X}^I). \quad (11)$$

Thereby, the interpolant and its weights N^I have to fulfill several basic properties:

- *partition of unity*: the sum over all interpolation weights equals one

$$\sum_I N^I = 1,$$

- *nodal function value interpolation*: the evaluation of the interpolant at given node locations \mathbf{X}^J provides the corresponding nodal value, thus

$$N^I(\mathbf{X}^J) = \delta_{IJ},$$

- *smoothness*: the derivatives of the interpolant exist,

$$\exists \frac{\partial N^I}{\partial \mathbf{X}},$$

- *linear completeness*: The interpolant exactly reproduces linear functions in the domain.

As already shown in Sec. 1, various approaches for 3D interpolants exist, which are often limited to simple corner connectivities. For our aim to construct efficient finite elements in 3D, two drawbacks exist: first, those 3D interpolants are very expensive in comparison with usual interpolants used for standard elements like trilinear shape functions for a hexahedron, and they are often limited to simple corner connectivities.

4.2. Extension of Malsch interpolant to convex three-dimensional domains

Our interpolant shall also be suitable for complex corner connectivities and we therefore refer to the 2D interpolant proposed by Malsch et al. [10] that is the foundation for our extension to 3D. It provides a generally applicable interpolant for any polyhedron with any internal facet and nodal configuration.

For the interpolant, we resort to geometric measures that are arranged in functions that are zero or minimal on facets or nodes. Those minimum functions are then combined to define linearly independent interpolants. The needed measures are all of geometric nature and can be classified as invariant measures inside the polyhedral domain (facet area A^F , nodal volume contribution k^I) and variable measures depending on the evaluation point (point-to-facet volume r^F).

The interpolation at the interior point \mathbf{X} is defined on the discrete nodal data and geometric measures. It can be generally established as

$$N^I(\mathbf{X}) = \frac{k^I s^I(\mathbf{X})}{\sum_J k^J s^J(\mathbf{X})} \quad (12)$$

with the auxiliary boundary functions $s^I(\mathbf{X})$ and the constants k^I . The purpose of the functions s^I is the consideration of the boundary behavior: for an evaluation on a boundary facet F , (11) merely depends on all N^I of the adjacent nodes to F . Otherwise all weights of non-adjacent nodes vanish. Thus, s^I can be constructed as

$$s^I(\mathbf{X}) = \prod_{F \notin \mathcal{F}^I} r^F(\mathbf{X}) \quad (13)$$

with the product of different facet functions r^F where each vanishes on its associated facet F . With the conditions $k^I > 0$ and $r^F \geq 0$, (12) renders a smooth and bounded interpolation. Besides this, the only restrictions for r^F are C^∞ continuity inside the domain and C^0 continuity on its boundaries.

To specify this general approach for convex 3D polyhedra, the constant k^I is the nodal volume contribution that is defined by the volume of the convex hull of the node with its adjacent nodes $\Delta^I(\mathcal{F}^I)$, see Fig. 4b, as

$$k^I = \kappa^I \Delta^I(\mathcal{F}^I), \quad (14)$$

where κ^I penalizes the nodal cardinality by

$$\kappa^I = \left[\frac{1}{n^I} \right]^3. \quad (15)$$

Furthermore, the point-to-facet volume can be used as the facet function r^F in (13), see Fig. 4c. Introducing the abbreviations

$$b^I := \frac{k^I s^I}{\prod r^F} = \frac{k^I}{\prod_{F \in \mathcal{F}^I} r^F} \quad (16)$$

only in terms of adjacent entities, (12) may be re-written as

$$N^I(\mathbf{X}) = \frac{b^I(\mathbf{X})}{\sum_J b^J(\mathbf{X})}. \quad (17)$$

On convex simple polyhedra, b^I corresponds to the definition of the barycentric coordinates in [25]. In contrast to (12), this simplification is not valid on the boundary where the denominator of (16) equals zero.

4.3. Analytic derivatives

For our interpolant we can directly compute the derivatives and do not need approximative finite difference approximations. With (17) the derivatives are given by:

$$\frac{\partial N^I}{\partial \mathbf{X}} = \frac{\frac{\partial b^I}{\partial \mathbf{X}} \sum_J b^J - \left[\sum_J \frac{\partial b^J}{\partial \mathbf{X}} \right] b^I}{\left[\sum_J b^J \right]^2}, \quad (18)$$

where with the gradient of b^I follows

$$\frac{\partial b^I}{\partial \mathbf{X}} = -b^I \frac{\sum_{F \in \mathcal{F}^I} \left[\frac{\partial r^F}{\partial \mathbf{X}} \prod_{G \in \mathcal{F}^I \setminus F} r^G \right]}{\prod_{F \in \mathcal{F}^I} r^F}. \quad (19)$$

The derivative of the volume $\frac{\partial r^F}{\partial \mathbf{X}}$ can be computed by the decomposition into tangential and normal directions with respect of the facets' orientation, see Fig. 4c. Therefore, we obtain with Cavalieri's principle for the pure volume shearing in tangential directions \mathbf{t}_i^F

$$\frac{\partial r^F}{\partial \mathbf{t}_i^F} = 0. \quad (20)$$

With a Taylor expansion in normal direction

$$r^F(\mathbf{X} + d\mathbf{n}^F) = r^F(\mathbf{X}) + \frac{\partial r^F}{\partial \mathbf{n}^F} d\mathbf{n}^F + \mathcal{O}^2, \quad (21)$$

the known pyramidal volume definition and the facet area A^F , we can identify the derivative of the facet volume function in normal direction as

$$\frac{\partial r^F}{\partial \mathbf{n}^F} = \frac{A^F}{3} \mathbf{n}^F, \quad (22)$$

which consistently applied in (19) and (18) leads to the overall derivative $\frac{\partial N^I}{\partial \mathbf{X}}$ in terms of the local facet's $[\mathbf{n}^F, \mathbf{t}_1^F, \mathbf{t}_2^F]$ -coordinate system which can easily be mapped to the global coordinate system.

4.4. Interpolation examples

To test the constructed interpolant, we apply it to two different examples. The first domain is a regular hexahedron, Fig. 5. Figure 5a shows the results for shape function N^6 and the corresponding derivative plot, Fig. 5b, where the arrows are indicating both the direction of the maximal ascends and the magnitude by its size. Compared with the trilinear analytic shape functions merely rounding errors have been observed both for the shape function and its derivative (normalized error $\varepsilon \ll 10^{-15}$).

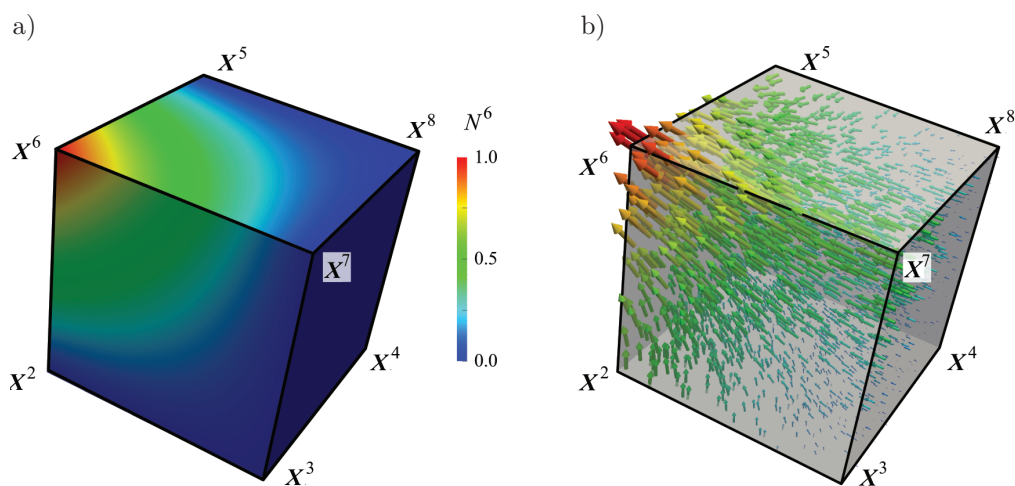


Fig. 5. Interpolants and gradients inside a simple hexahedron: a) interpolant N^6 , b) gradient $\frac{\partial N^6}{\partial \mathbf{X}}$.

The second example deals with the mentioned arbitrariness regarding the complexity of the polyhedron: The given pyramid, Fig. 6, with a quadratic bottom facet is complex due to the four

adjacent facets to the top node X^5 . The shown interpolant is also suitable for this group of polyhedra: although no analytic comparative statement is available, the interpolant (a) and its derivative (b) show a good behavior for qualified points. However, it does not fulfill the linear completeness criterion exactly – for the investigation of the linear edge behavior on edges connected to complex nodes (the observed maximal normalized error was below five percent) – as the formulation itself does not imply this. Nevertheless, accepting this slight restriction for complex and without any restriction for non-complex polyhedra, we can proceed to use the interpolant for our polyhedral domains.

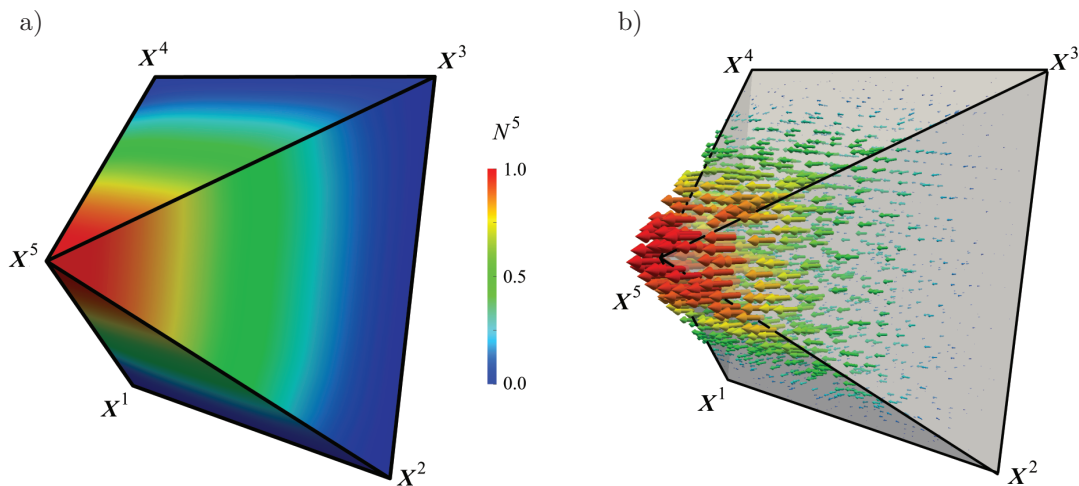


Fig. 6. Interpolants and gradients inside a complex pyramid: a) interpolant N^5 , b) gradient $\frac{\partial N^5}{\partial \mathbf{X}}$.

5. POLYHEDRAL FINITE ELEMENTS

With our proposed three-dimensional interpolant on arbitrary convex polyhedra we have obtained for each polyhedral element access to (8) and (9) where the interpolants N^I and their derivatives $N^I_{,i}$ on Ω_e are essential. We can now devise a finite element formulation, where, at this stage, an adequate quadrature strategy for the element domains Ω_e is still missing.

5.1. Polyhedral interpolation

One possibility is based on the proposal by Sukumar [18, 21] extended to three dimensions. The basic idea to handle each polyhedral domain Ω_e is its decomposition into tetrahedral subdomains $\bar{\Omega}_e$. To obtain an adequate decomposition of the polyhedral domain, an auxiliary node is defined with (17) by

$$\bar{\mathbf{X}}^A = \sum_I N^I(\bar{\mathbf{X}}^A) \mathbf{X}^I, \quad (23)$$

where the choice of the position inside the polyhedral is arbitrary, e.g., at the barycenter, which usually leads to a good Delaunay tessellation for the union of global and auxiliary nodes.

On the resulting tetrahedral subdomains, known quadrature rules like a Gaussian quadrature can be used for the integration of a function f ,

$$\int_{\bar{\Omega}_e} f \, d\bar{\Omega}_e = \sum_G f(\bar{\mathbf{X}}^G) \bar{w}^G. \quad (24)$$

The mapping $\mathbf{J} = [\bar{\mathbf{X}}_1 \mid \bar{\mathbf{X}}_2 \mid \bar{\mathbf{X}}_3]$ with the physical element's affine basis vectors $\bar{\mathbf{X}}_i$ along the edges of the physical subdomain $\bar{\Omega}_e$ projects the generic Gaussian quadrature points, given in the Cartesian ξ_i -coordinates, to the points $\bar{\mathbf{X}}^G$ in $\bar{\Omega}_e$ with their modified weights $\bar{w}^G = |\mathbf{J}|w^G$, Fig. 7. To express the physical integration point as weighted nodal coordinates, the proposed polyhedral interpolant (12) can be used for any convex polyhedral shape. This directly leads to a polyhedral element stiffness according to (9) in terms of the global polyhedral nodes' displacements.

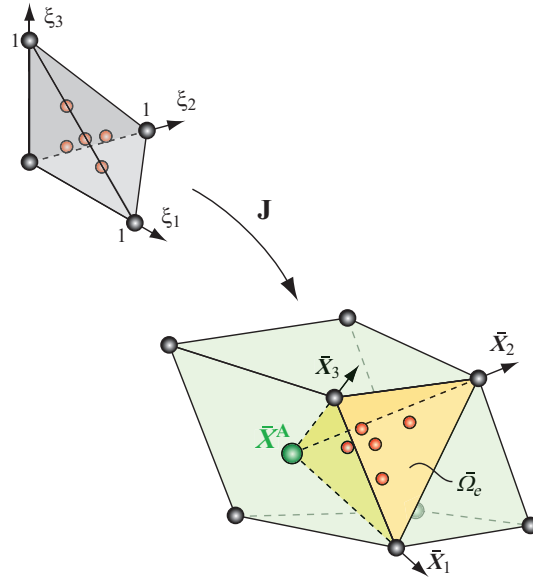


Fig. 7. Mapping of quadrature point into physical polyhedral element.

5.2. Subelement technique

For comparison reasons we resort – besides standard hexahedral element formulations for adequate (regular) meshes – to a subelement technique that uses the same basic idea of a domain decomposition, but now not only for integration reasons but for a complete tetrahedral submesh. We again introduce an auxiliary internal node $\bar{\mathbf{X}}^A$ that is interpolated by the global nodes by (23). With the use of isoparametric concept, the displacement field at the auxiliary node is analogously constrained,

$$\bar{\mathbf{u}}^A = \sum_I N^I(\bar{\mathbf{X}}^A) \mathbf{u}^I. \quad (25)$$

Based on this set of global and auxiliary nodes inside the polyhedron, a tetrahedral submesh can be established within the polyhedron by a common Delaunay tessellation, with the known linear tetrahedral shape functions

$$\begin{aligned} \bar{N}^1 &= 1 - \xi_1 - \xi_2 - \xi_3, \\ \bar{N}^2 &= \xi_1, \\ \bar{N}^3 &= \xi_2, \\ \bar{N}^4 &= \xi_3, \end{aligned} \quad (26)$$

here given in the generic coordinate $\bar{\mathbf{x}}$ system, can be used for a local interpolation inside the submesh alternative to (17); in this context (\star) indicated variables on this submesh.

With the auxiliary internal node being part of the submesh, this procedure would affect the solution of the global system of equation as the size of the global stiffness matrix is increased by non-polyhedral node entities. Otherwise the direct calculation of a local polyhedral stiffness matrix like

$$\begin{bmatrix} \overline{\mathbf{K}}_T^{II} & \overline{\mathbf{K}}_T^{IA} \\ \overline{\mathbf{K}}_T^{AI} & \overline{\mathbf{K}}_T^{AA} \end{bmatrix} \begin{bmatrix} \mathbf{u}^I \\ \overline{\mathbf{u}}^A \end{bmatrix} = \begin{bmatrix} \overline{\mathbf{f}}^I \\ \overline{\mathbf{f}}^A \end{bmatrix}, \quad (27)$$

with a subsequent static condensation of the entities on the global nodes is possible. On the subelements we can then obtain the residual vector $\mathbf{f}_{\text{int}}^I$ and the corresponding tangential stiffness matrix \mathbf{K}^{IJ} that is only depending on the nodes of our global finite element system, that can be assembled and solved like any other domain. This approach reduces the numerical efforts for polyhedral interpolation to a minimum as (17) has only be evaluated once and also this interpolation piecewise satisfies the interpolation properties from Subsec. 4.1.

6. NUMERICAL EXAMPLES

In the following sections, our proposed element formulations shall be verified and tested on several examples. The formulation with polyhedral interpolation (according to Subsec. 5.1) will be indicated as PI elements. The formulation with tetrahedral subelements is termed SE element. For comparison, trilinear hexahedral standard elements H8 and locking free hexahedral elements H8_{lf} with reduced integration and hourglass stabilization proposed by Reese [12] have been used. As material model we used, for our examples, a non-linear Neo-Hookean material model with the stored energy density function

$$W(\mathbf{C}) = \mu \mathbf{I} + \left[\lambda I_3 - \sqrt{I_3} - \mu \right] \mathbf{C}^{-1}. \quad (28)$$

Here the Cauchy-Green deformation tensor follows as $\mathbf{C} = \mathbf{F}^T \mathbf{F}$, its third invariant I_3 and the Navier-Lamé material constants are μ and λ .

6.1. Cook's membrane based on regular mesh

As the described polyhedral finite element formulations are completely independent of the real polyhedron's shape, we can also verify our element types by a comparison with a standard element mesh.

We consider the classical Cook's membrane (see Fig. 8a, thickness 1 mm) which is fixed on the left hand side and loaded with a distributed vertical load where $\sum F = 250$ N. The Navier-Lamé constants are given by $\mu = 80.194$ N/mm² and $\lambda = 120.291$ N/mm² and the whole domain is meshed by a $n \times n \times 1$ hexahedral mesh. The reference result for the vertical displacement of the right tip R is $u_{3,\text{Ref}}^R = 16.0 \cdot 10^{-3}$ mm [13].

Figure 8b shows the result of a convergence study normalized to the reference result for different meshing parameters n and the different element formulations. It can be seen that the polyhedral interpolated PI elements provide the same system response as the trilinear hexahedral H8 elements. Otherwise the SE elements shows a good and even better behavior for technically relevant mesh refinements. All polyhedral formulation show a good convergence for denser meshes and also obvious, all formulations are not yet competitive with advanced standard element formulations like the H8_{lf} element. Regarding the computational costs, we examine the relative CPU times of each formulation normalized to the H8 CPU time (Table 1, column 2) and the operation distributions on three categories ('geometric', 'quadrature', 'overhead', columns 3–5). The PI elements with analytic derivatives have a tremendously high τ_{rel} slightly below 150 due to plenty geometric operations inside the necessary and sumptuous implementation of (17). Otherwise the SE elements are fast,

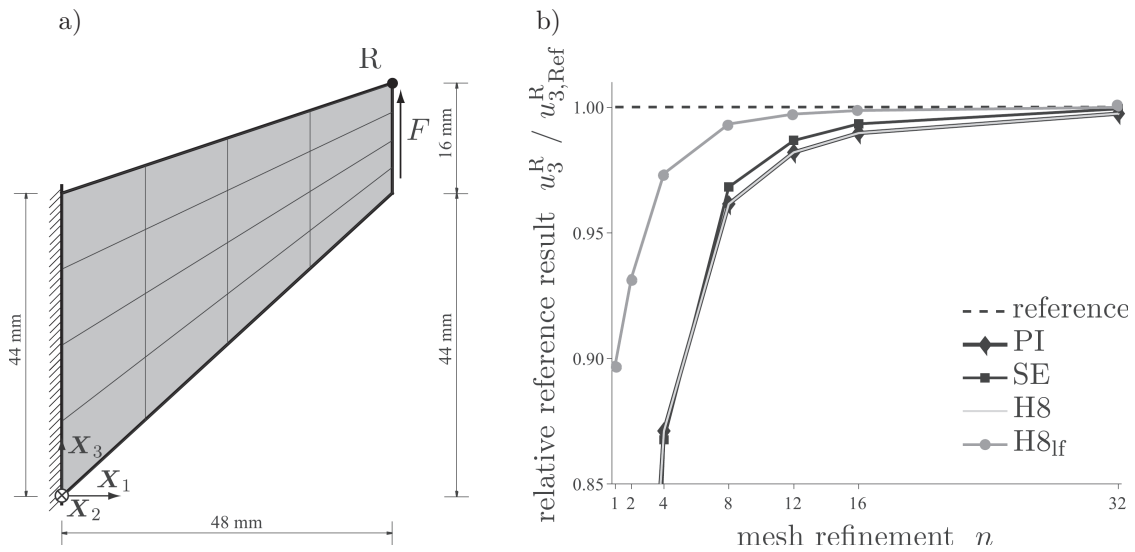


Fig. 8. Cook's membrane: a) problem description ($n = 4$), b) convergence study for different element types.

Table 1. Relative CPU time τ_{rel} and operation distribution for proposed element types and trilinear hexahedral element.

element	τ_{rel}	geometric	quadrature	overhead
PI	144	96%	3%	1%
SE	15	71%	27%	2%
H8	1	62%	30%	8%

but their numerical result suffer from general (distorted) meshes, see next section, but a great sensitivity considering the choice of the auxiliary node $\bar{\mathbf{X}}^A$ is not neglectable and has to be examined in future works.

6.2. Polyhedral examples on arbitrary meshes

The comparison with the classical Cook's membrane does not cover the whole scope of the element abilities and thus we want to demonstrate, in the following section, their powerful possibilities with some real polyhedral examples.

6.2.1. Cantilever

Our first example shows the abilities of our elements: we still have the very simple domain geometry of a cantilever (dimensions $10 \times 1 \times 1$ m, Neo-Hookean material model (28), Young's modulus $Y = 4 \cdot 10^6$ N/mm², Poisson ratio $\nu = 0.3$) which is clamped on the left side and loaded with a vertical line load p on the right top line, but the underlying mesh consists of highly irregular polyhedra. The polyhedral mesh consist of 126 elements that were constructed by Voronoi cells around 126 randomly distorted seed points which leads in the presented example to 649 nodes with the distribution of nodes per elements (shown in Fig. 9) which cover the range from 8 to 34 nodes per element. In the technical realization, the freeware tool *TetGen* [15] has been used for the Delaunay tessellation and the initial generation of its dual Voronoi cells. In this constructed mesh, the individual grain sizes may be controlled by the seed point locations and are comparable to structural height of for example a μ -device.

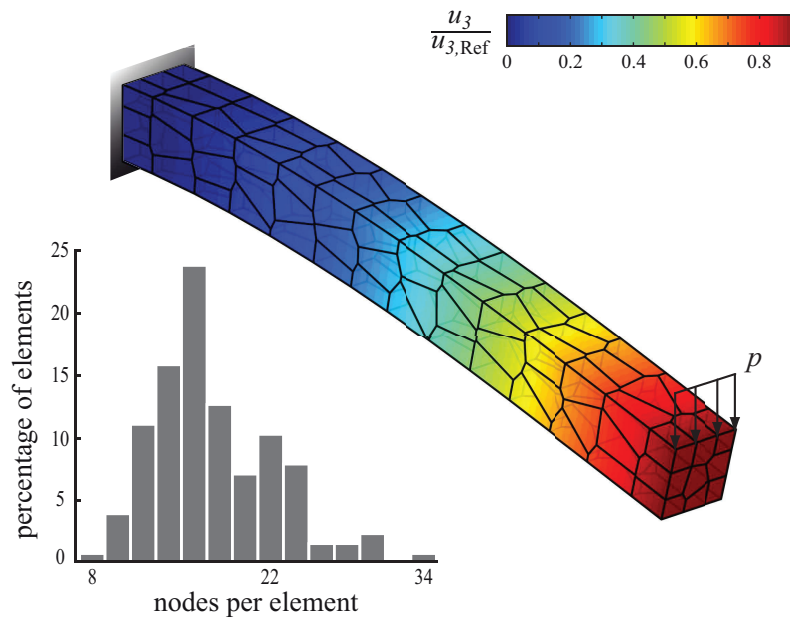


Fig. 9. Deformed polyhedral cantilever colored by u_3 -displacement magnitude with nodes-per-element histogram.

To enable a comparison to an analytic result, we limit the vertical line load $p = 100$ N/m to the scope of linear elasticity: the analytic vertical reference displacement at the front tip of this Bernoulli beam is then $u_{3,Ref} = 1.0 \cdot 10^{-3}$ m. For the shown example, we obtain a good numerical and mechanical performance with respect to the element count (Fig. 9) for the PI elements. The SE elements suffer massive locking effects, which urges future investigations or an improved mixed variational formulation on the submesh.

6.2.2. Truncated cuboctahedra and icosahedra structures

Our final examples for our polyhedra now also have a polyhedral or very complex domain, where by each subdomain that originally belongs to an arbitrary grain or crystal is also meshed as one polyhedral element. Unfortunately, we are losing the possibility to compare numerical and analytic results.

The first arrangement consists of 9 elements with 240 nodes, where the ball-shaped elements represent a 48 node omnitruncated cuboctahedron element each (characteristic cell dimension 1 mm) that appear in nature, e.g., as crystal morphology of galena (Pb_2S). The spherical elements are linked by 12 node prisms (average edge dimensions 0.7 mm, material properties for all elements: Young's modulus $Y = 4 \cdot 10^6$ N/mm², Poisson ratio $\nu = 0.3$). The upper face is loaded by constant and uniform pressure distribution ($p = 100$ N/mm²) and the outer element nodes on the bottom are beared floatingly, Fig. 10a.

The second generic example are 15 icosahedra (characteristic edge length 0.1 mm, Young's modulus $Y_1 = 4 \cdot 10^6$ N/mm², Poisson ratio $\nu = 0.3$) bridged by 28 octahedra (same properties as icosahedra except Young's modulus $Y_2 = 2Y_1$) with concentrated tangential forces at the shown nodes on the top satellite elements ($\sum F = 12$ N) and fixed bearings on the bottom nodes near the rotational axis, Fig. 10b.

Each of these two examples shows expected mechanical responses, and we want to emphasize, that although they only consists of polyhedral elements the developed formulations have no effect on the surrounding finite element framework, thus any combinations and complications with other element types (like mixed meshes with standard elements) and other topics beyond pure nonlinear elasticity (like zero-thickness contact elements at the elements' interfaces) are allowed and possible.

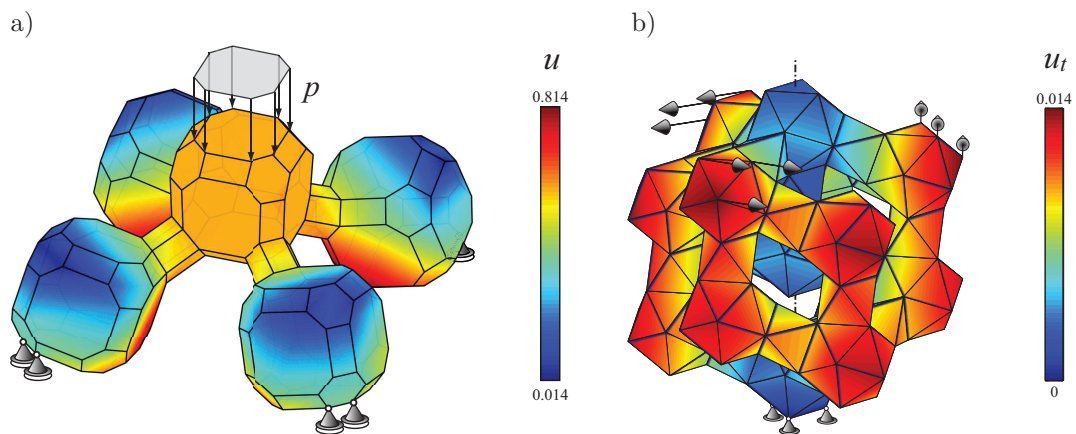


Fig. 10. Polyhedral structures: a) deformed truncated cuboctahedra structure bridged by prisms loaded by top pressure p and floatingly beared on bottom (color corresponds to displacement magnitude), b) deformed 28 icosahedra linked by 15 octahedra loaded by tangential loads and fixed at central bottom nodes (color indicating tangential displacement).

7. CONCLUSION

With respect to arbitrary convex polyhedral elements, we have proposed a general 3D interpolant and used it for the construction of two different finite element formulations for convex polyhedra in nonlinear continuum mechanics that are compatible with the common finite element framework. As has been demonstrated, easy discretization of polyhedral structures is possible due to a complete shape independence which extends the standard element shapes significantly. The three-dimensional interpolant provides good numerical results but suffers from high computational costs especially for many expensive geometric operations. We showed a modified interpolation strategy that enables us to decrease the CPU times but that is accompanied with unfavorable limitations in the mechanical responses.

The presented element formulations are very prolific for general arbitrary meshes and have still development potential. Therefore, the usage of mixed variational principles has to be considered. Also the extension of the underlying nonlinear elastic Neo-Hookean to general ortho- and anisotropic material models for the simulation of directional material properties by, e.g., sheet rolling processes is desirable.

REFERENCES

- [1] V.V. Belikov, V.D. Ivanov, V.K. Kontorovich, S.A. Korytnik, A.Y. Semenov. The non-Sibsons interpolation: A new method of interpolation of the values of a function on an arbitrary set of points. *Comput. Math. Math. Phys.*, **37**(1): 9–15, 1997.
- [2] A. Constantiniu, P. Steinmann, T. Bobach, G. Farin, G. Umlauf. The adaptive Delaunay tessellation: a neighborhood covering meshing technique. *Comput. Mech.*, **42**(5):655–669, 2008.
- [3] G. Dasgupta. Interpolants within convex polygons: Wachspress shape functions. *J. Aero. Eng.*, **16**: 1–8, 2003.
- [4] M. Floater. Mean value coordinates. *Comput. Aided Geomet. Des.*, **20**: 19–27, 2003.
- [5] M. Groeber, S. Ghosh, M.D. Uchic, D.M. Dimiduk. Developing a robust 3-D characterization-representation framework for modeling polycrystalline materials. *J. Miner. Met. Mater. Soc.*, **59**(9): 32–36, 2007.
- [6] M.A. Groeber, B. Haley, M.D. Uchic, D.M. Dimiduk, S. Ghosh. 3D reconstruction and characterization of polycrystalline microstructures using a FIB-SEM system. *Mater. Char.*, **57**(4–5): 259–273, 2006.
- [7] H. Hiyoshi, K. Sugihara. Another interpolant using Voronoi diagrams. *IPSS SIG Notes*, **98-A1-62**: 33–40, 1998. In Japanese.
- [8] K. Hormann, M.S. Floater. Mean value coordinates for arbitrary polygons. *ACM Trans. Graph.*, **25**(4): 1424–1441, 2006.
- [9] Y. Lipman, D. Levin, D. Cohen-Or. Green coordinates. *ACM Trans. Graph.*, **27**:78: 1–10, 2008.
- [10] E.A. Malsch, J.J. Lin, G. Dasgupta. Smooth two dimensional interpolations: A recipe for all polygons. *J. Graph. Tool*, **10**(2): 27–39, 2005.

-
- [11] M. Meyer, H. Lee, A. Barr, M. Desbrun. Generalized barycentric coordinates on irregular polygons. *J. Graph. Tool*, **7**: 13–22, 2002.
- [12] S. Reese. A large deformation solid-shell concept based on reduced integration with hourglass stabilization. *Int. J. Numer. Meth. Eng.*, **69**: 1671–1716, 2007.
- [13] S. Reese, M. Küssner, B. Reddy. A new stabilization technique for finite elements in non-linear elasticity. *Int. J. Numer. Meth. Eng.*, **44**: 1617–1652, 1999.
- [14] M. Sambridge, J. Braun, H. McQueen. Geophysical parameterization and interpolation of irregular data using natural neighbours. *Geophys. J. Int.*, **122**: 837–857, 1995.
- [15] H. Si. *TetGen – A quality tetrahedral mesh generator and three-dimensional Delaunay triangulator*. Weierstrass Institute for Applied Analysis and Stochastics, Berlin, 1.4 edition, 01 2006.
- [16] R. Sibson. A vector identity for the Dirichlet tessellation. *Math. Proc. Camb. Phil. Soc.*, **87**(1): 151–155, 1980.
- [17] R. Sibson. A brief description of natural neighbor interpolation. In V. Barnett, editor, *Interpreting Multivariate Data*, chapter 2, pages 21–36. Wiley, Chichester, 1981.
- [18] N. Sukumar, E.A. Malsch. Recent advances in the construction of polygonal finite element interpolants. *Arch. Comput. Meth. Eng.*, **13**(1): 129–163, 2006.
- [19] N. Sukumar, B. Moran, T. Belytschko. The natural element method in solid mechanics. *Int. J. Numer. Meth. Eng.*, **43**: 839–887, 1998.
- [20] N. Sukumar, B. Moran, A.Y. Semenov, V.V. Belikov. Natural neighbor Galerkin methods. *Int. J. Numer. Meth. Eng.*, **50**: 1–27, 2001.
- [21] N. Sukumar, A. Tabarraei. Conforming polygonal finite elements. *Int. J. Numer. Meth. Eng.*, **61**(12): 2045–2066, 2004.
- [22] L. Traversoni. Modified natural neighbor interpolant. *Proceedings of SPIE*, **1830**: 196–203, Nov. 1992.
- [23] N. Uhlmann, J. Pavlovic, M. Hilbinger, M. Salamon, F. Nachtrab, R. Bähr, F. Mních, R. Hanke. Fast 3D-analysis of texture features – Possibilities of high resolvent X-ray computer tomography in the analysis of texture features of metallic material. *VDI Reports*, **2061**: 81–89, 2009 (In German).
- [24] E.L. Wachspress. *A rational finite element basis*. Number 114 in Mathematics in Science and Engineering. Academic Press, New York, 1975.
- [25] J. Warren. Barycentric coordinates for convex polytopes. *Adv. Comput. Math.*, **6**: 97–108, 1996.
- [26] J. Warren. On the uniqueness of barycentric coordinates. *Contemp. Math.*, **334**: 93–99, 2003.
- [27] J. Warren, S. Schaefer, A.N. Hirani, M. Desbrun. Barycentric coordinates for convex sets. *Adv. Comput. Math.*, **27**: 319–338, 2007.
- [28] D. Watson. Compound signed decomposition, the core of natural neighbor interpolation in n-dimensional space, 2001.
- [29] S. Weißer. Residual error estimate for BEM-based FEM on polygonal meshes. *Numer Math.*, **118**: 765–788, 2011.